J Mater Sci (2008) 43:1939–1947
DOI 10.1007/s10853-008-2461-0

Supercritical CO_2 processing of polymers for the production of materials with applications in tissue engineering and drug delivery

Ana M. López-Periago · Arlette Vega · Pascale Subra · Anna Argemí · Javier Saurina · Carlos A. García-González · Concepcion Domingo

Received: 13 November 2007 / Accepted: 8 January 2008 / Published online: 30 January 2008

Abstract Supercritical carbon dioxide ($SCCO_2$) was used for the preparation of foamed sponges and intermingled fibers of biopolymers with potential applications in tissue engineering and drug delivery. The work was focused on the processing of both biodegradable polylactic acid (L-PLA) and non-biodegradable polymethylmethacrylate (PMMA) homopolymers. Monolithic porous sponges of amorphous PMMA were prepared using $SCCO_2$ as a porogen agent by simple swelling and foaming. Under similar experimental conditions, L-PLA was crystallized. The study also addresses the impregnation of biopolymers with an active agent dispersed in $SCCO_2$. The drug used for impregnation was triflusal, a platelet antiaggregant inhibitor for thrombogenic cardiovascular diseases. Foaming often leads to a closed pore structure after depressurization which is disadvantageous for 3D scaffolds as it does not fulfill the requirement of interconnectivity necessary for cell migration. To overcome these drawbacks, fibers forming macroporous structures were prepared using a semicontinuous antisolvent (SAS) technique.

A. M. López-Periago (✉) · C. A. García-González · C. Domingo
Instituto de Ciencia de Materiales de Barcelona, CSIC, Campus UAB, 08193 Bellaterra, Spain
e-mail: conchi@icmab.es; amlopez@icmab.es

A. Vega · P. Subra
Laboratoire d'Ingénierie des Matériaux et des Hautes Pressions, C.N.R.S., Institut Galilée, Université Paris 13, 99 Avenue Jean Baptiste Clément, 93430 Villetaneuse, France

A. Argemí · J. Saurina
Department of Analytical Chemistry, University of Barcelona, Diagonal 647 08028 Barcelona, Spain

Introduction

Tissue engineering is evolving from the use of implants that replace damaged parts, to the use of 3D scaffolds that induce the formation of new functional tissues [1–4]. Many polymeric materials, from biodegradable to biostable, are being evaluated for a possible role in tissue engineering. The architecture of the scaffold also plays an important role in modulating the response behavior of cultured cells. Required characteristics for a correct architecture include high porosity and an interconnected 3D macroporous network necessary for cell proliferation [5–9]. Scaffolds can take forms ranging from microcellular structures to networks of fibers. Moreover, well-developed polymeric porous structures facilitate their usage as drug delivery systems due to their high surface area and blood circulation efficiency [4, 10].

Technology based on supercritical carbon dioxide ($SCCO_2$) is generally proposed as an alternative to overcome some of the problems associated with the use of traditional organic solvents for pharmaceuticals and biomaterials preparation [11, 12]. $SCCO_2$ is a clean solvent and has a low critical temperature ($T_c = 304.2$ K) and a moderate critical pressure ($P_c = 7.3$ MPa). In supercritical processing, the $SCCO_2$ solvent is often used to alter the properties of the matrix so as to deliver an ingredient for impregnation or reaction, depending on the destined purpose. The changes in properties utilized include softening, swelling, plasticization, changes in solubility, depression in glass transition or melting temperature, changes in surface tension or in pore structure, etc. In the specific case of polymers, many of the applications exploit the fact that $SCCO_2$ is an excellent non-solvating porogenic agent for amorphous polymers while being a poor solvent [13, 14]. It is used to produce polymer foams by pressure-induced phase separation [15–18] and for impregnation [19–23].

Furthermore, spray processes involving $SCCO_2$ have achieved considerable success in addressing polymer particles and fibers production [24–28].

The first objective of the current study is to explore $SCCO_2$ processing technology possibilities in the production of morphologically different porous systems (foamed sponges and networks of fibers) of biodegradable L-PLA (L-polylactic acid) and non-biodegradable PMMA (polymethylmethacrylate). Solid monolithic porous scaffolds were prepared by simple swelling and foaming with $SCCO_2$. Fibers were prepared using the SAS technique (precipitation with a compressed fluid antisolvent). As a final point, this work also addresses the interaction of $SCCO_2$-drug (triflusal) solutions with semicrystalline L-PLA and amorphous PMMA.

Materials and methods

Materials

2-acetyloxy-4-(trifluoromethyl)benzoic acid or triflusal (kindly donated by Uriach S.A.) was chosen as the organic solute to be impregnated. The selected polymeric matrixes were PMMA beads (from Bonar Polymers Ltd, ~500,000 Da) and L-PLA pellets (kindly donated by Purac, ~350,000 Da). Dichloromethane (DCM, HPLC grade, Prolabo) and CO_2 (99.5 wt.%, Air Liquide) were the used fluids.

Process and equipment

The experimental tests were carried out with two objectives, either the production of monolithic foams or the precipitation of fibers.

Batch equipment for polymers foaming/impregnation

Experiments were performed in a high-pressure equipment running in the batch mode (Fig. 1a). In a typical experiment, the autoclave (TharDesign, 70 mL) was charged either with 1 g of polymer (L-PLA or PMMA) for foaming experiments or 0.5 g of polymer and 0.5 g of triflusal for impregnation experiments. For the latter, triflusal particles were first wrapped in cylinders made of 0.45 μm pore filter paper. The cylinders were physically separated of the PMMA in the vessel by a distance of 2–3 cm. Then, $SCCO_2$ was added and the system was maintained at fixed pressure and temperature during 24 h. The reactor was heated using resistances. The CO_2 was pressurized with a syringe pump (TharDesign SP240). The system was stirred at 300 rpm. Recovered samples containing triflusal were washed with ethanol.

Semicontinuous equipment for polymer fibers precipitation

The SAS experiments were conducted in the apparatus shown schematically in Fig. 1b, operated in a semicontinuous mode. The spray chamber consisted on a high-pressure vessel (1, Autoclave Engineers) of 5 cm i.d. ×25 cm long, with sapphire windows (2) at three different levels. The CO_2 was first cooled (3) and then pumped using a reciprocating pump (4, Lewa EK3). Prior to entering the precipitation chamber, the gas was preheated at the working temperature. The pressure inside the vessel was controlled downstream (5) with a micrometering valve (7), and the temperature was controlled by heating jackets. DCM solutions of polymer were sprayed into the precipitation chamber using a reciprocating dual-piston minipump (8, Milton Roy LDC). In a typical experiment, once the temperature of the vessel had attained the desired value (313 K), the CO_2 was introduced through a 1/8″ tubing keeping valve (6) closed, until the desired pressure was reached (11 MPa). Then, valve (6) was opened and the system was allowed to equilibrate maintaining the CO_2 flow at a fixed value (ca. 100 mL min^{-1}). The polymer solution was introduced into the precipitation chamber

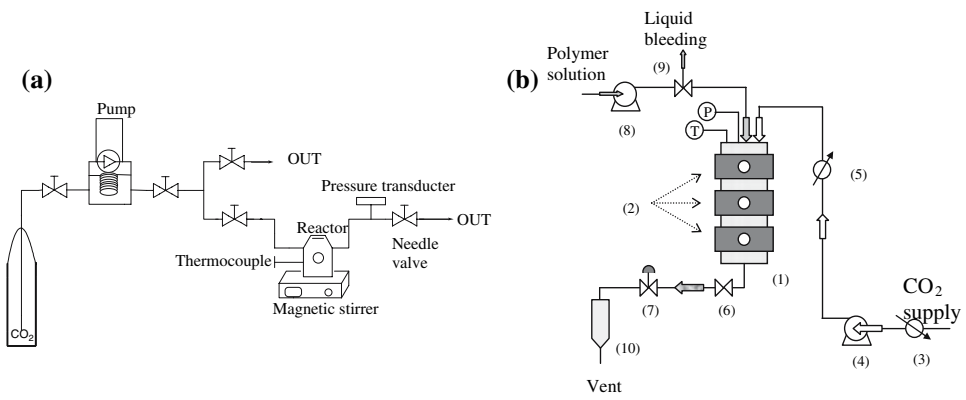

Fig. 1 High-pressure equipment: (**a**) batch and (**b**) semicontinuous SAS

through a 100 μm diameter conical spray (swirl) nozzle at a liquid flow rate of 3 mL min^{-1}. At the bottom of the vessel, the precipitated polymer was collected on a membrane filter placed on top of a stainless steel frit of 2 μm porosity. When the polymer precipitation was finished, the system was depressurized across a metering valve and the liquid recovered in a cyclone (10). The precipitated polymer was dried with CO_2 flow.

Characterization

The composition of processed samples was determined by proton nuclear magnetic resonance (^{1}H NMR, Bruker ARX-300 NMR spectrometer) in deuterated chloroform. Micrographs were obtained by using a scanning electron microscope (SEM, JEOL JSM-840). The glass and/or melting temperatures of polymers were measured on a differential scanning calorimeter (DSC-822e/400 Mettler Toledo). Thermograms were obtained at a heating rate of 10 K min^{-1} in the range 293–573 K under N_2 purge. A Nano Indenter XP testing machine from MTS Nano Instruments was used to acquire samples mechanical data (hardness) on the submicron scale. Testing based on pyramidal Berkovich tips was conducted at room temperature. Each measured data was an average of 10 indents. Materials were loaded to a maximum load of approximately 100 mN.

For PMMA/triflusal system, drug release in water was spectrophotometrically monitored over time at 310 K under stirring (accelerated delivery) and at a pH value of 2 (0.01 M HCl) in order to simulate the stomach physiological conditions. A continuous flow system consisting of a peristaltic pump (Watson Marlow 505DU) for recirculation of the solution and a UV spectrophotometer (Perkin-Elmer Lambda-19) were used. Delivery profiles were recorded at 225 nm using a Helma flow-cell of 10 mm path length and 60 μL volume.

For L-PLA and PMMA fibers, the specific surface area (S_a) and pore volume (P_v) of prepared samples were determined by low-temperature N_2 adsorption, using an ASAP 2000 Micromeritics INC. Previous to measurements, samples were dried under reduced pressure (<1 mPa) at 323 K for 48 h. S_a was determined by the BET-method (Brunauer–Emmett–Teller) and P_v was estimated using the BJH-method (Barret–Joyner–Halenda).

Results and discussion

Microcellular foaming and impregnation

The type of polymers under investigation for $SCCO_2$ foaming was the amorphous PMMA and the semicrystalline L-PLA. Foaming was carried out in the high-pressure chamber described in Fig. 1a. The $SCCO_2$ preparation of microcellular foams can be decomposed into two steps [23, 29]. First, after an increase in temperature and pressure and upon polymer prolonged exposure to $SCCO_2$, saturation of the polymer by CO_2 is completed. Second, CO_2 is released leading to bubble nucleation induced by a thermodynamic instability. Pore growth then occurs and the microstructure can be controlled via the rate of pressure release.

For non-porous polymers, the impregnation process is based on polymer plasticization and swelling caused by CO_2, which facilitates the diffusion of impurities (residual monomer or solvent, initiator, etc.) to the fluid phase, and active agent infusion into the polymeric phase [30, 31]. For both, extraction and impregnation, solubility is the key aspect for achieving good results in a reasonable time using the minimum of extraction fluid and a processing system that can be constructed on a practical scale. The used active agent in this work, the triflusal, has a chemical structure similar to that of acetyl salicylic acid (ASA), the aspirin, but with an additional trifluoromethyl group. The replacement of hydrogen by fluorine in organic compounds often leads to a dramatic change in chemical and physical properties. For instance, fluorination has a pronounced effect on the interaction of the fluorinated molecule with the solvent and this often leads to remarkable changes in solubility. $SCCO_2$, in particular, is a solvent that exhibits a high degree of discrimination between solutes based on carbon/fluorine. Many studies have suggested that the Lewis acidic carbon atom of CO_2 interacts with a lone pair of electrons on fluorine in the C–F bond and renders the resultant fluorinated compound significantly soluble in $SCCO_2$ [14]. Measured solubility values of tirflusal in $SCCO_2$ at the working pressure and temperature were in the order of 3×10^{-2} mole fraction, which are 100-fold higher than those of ASA at similar pressures and temperatures. The impregnation of polymers upon contact with $SCCO_2$ solutions has been generally studied in the $SCCO_2$ flowing mode, where the impregnation process is governed by the amount of drug that can be carried by the mobile phase and the partition coefficient of the drug between the supercritical and polymer phases. As a first approach, the one-pass flow method was also used in this work to study the impregnation of triflusal in the polymers. For this specific system, the high solubility of triflusal on $SCCO_2$ led to the dissolution of a large amount of active agent from the extractor vessel that could not be loaded to the polymer in the impregnator vessel. As a consequence, large amounts of active agent were lost, even when working at very low flow rates of $SCCO_2$. Therefore, the $SCCO_2$ stagnant processing approach was used to study this specific system.

PMMA

The most relevant thermal phase change for amorphous polymers, such as PMMA, is the glass-to-rubber transition characterized by the glass transition temperature (T_g). The swelling and foaming behavior of PMMA films in presence of $SCCO_2$ have been widely described [32, 33]. Strong interactions between the PMMA and CO_2 molecules have been observed [34], which led to a dramatic T_g depression (333 K or more at the relatively low pressures of 4–6 MPa) [35, 36]. Based on the literature data [32–36], at the working conditions (20 MPa and 318 K) the PMMA adsorbed enough gas to lower its glass transition temperature below the processing temperature. Depressurization led to polymer vitrification when the glass transition temperature was reached. At this point, the structure could not grow further and was locked in with a specific morphology, and a uniform distribution of macropores throughout the polymer matrix has been described to be formed [33]. The $SCCO_2$ foaming process led to an integral foam structure with a microcellular core encased by a nonporous skin which resulted from rapid diffusion of the gas away from the surface. This is a trend already described in the literature for PMMA [37–39]. For the PMMA studied samples, SEM pictures showed no apparent external porosity in the beads after depressurization, making the internal pore volume nonaccessible (Fig. 2a, b). Under similar experimental conditions, impregnated PMMA particles showed spherical and pseudo-spherical geometry with dimensions between 50 and 100 μm of diameter (Fig. 2c) similar to that of the PMMA raw particles. SEM image revealed a collection of PMMA impregnated microspheres, without the presence of any surrounding crystals of triflusal.

The quantity of triflusal loaded in PMMA was estimated using ^{1}H-NMR spectroscopy (Fig. 3a). The spectra of the impregnated samples displayed all of the peaks corresponding to both the triflusal and the PMMA. The ^{1}H-NMR spectrum of the PMMA starting material revealed the

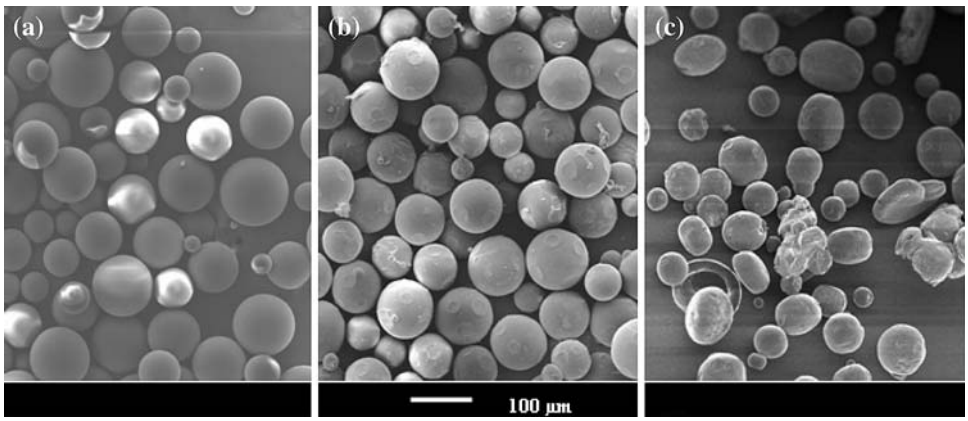

Fig. 2 SEM micrographs of (**a**) raw PMMA beads, (**b**) PMMA beads treated under $SCCO_2$ at 20 MPa and 318 K, and (**c**) PMMA beads impregnated with triflusal dissolved in $SCCO_2$ at 20 MPa and 318 K

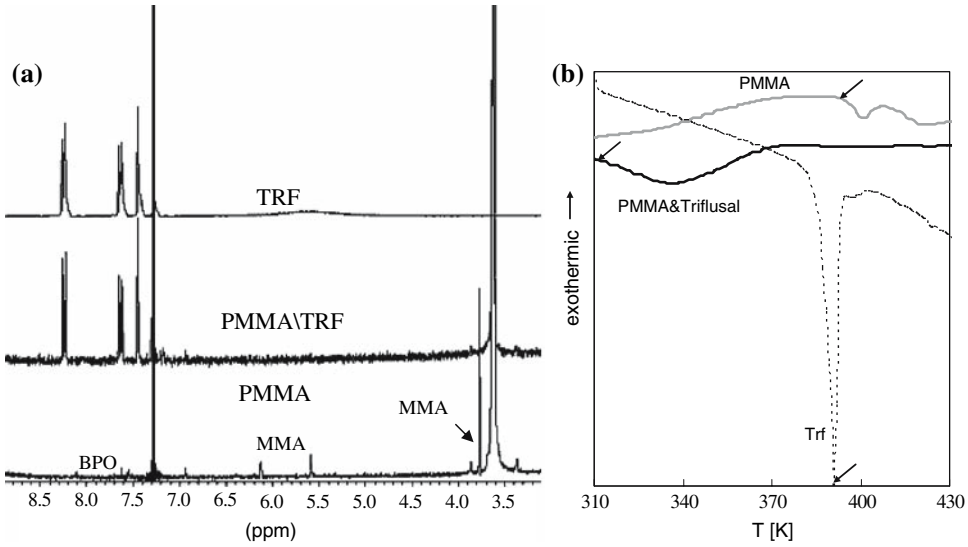

Fig. 3 Characterization of raw and triflusal impregnated PMMA at 20 MPa and 318 K by (**a**) ^{1}H-NMR and (**b**) DSC (arrows indicated the thermal transition)

peaks from the residual monomer methyl methacrylate (MMA) and the initiator benzoyl peroxide (BPO). These peaks disappeared from the impregnated system, exhibiting a purification of the polymer even when working in a batch $SCCO_2$ impregnation mode. The quantitative analysis indicated ca. 15 wt.% of triflusal in PMMA.

DSC analysis was performed to investigate the physical state of the drug in the particles, since this aspect could influence the release of the drug from the systems. Figure 3b shows the transitions obtained from DSC thermographs of the raw PMMA, raw triflusal, and impregnated PMMA with triflusal. The T_g of the raw PMMA, measured at the onset of the transition, appeared at 397 K. The triflusal presented a melting peak (T_m) at 390 K. For samples prepared by supercritical impregnation, no triflusal melting peak was observed even at the high loading of 15%, indicating that the triflusal was likely dispersed at a molecular level with the absence of crystallized triflusal. A remarkable reduction in the PMMA T_g to a value of $\sim$315 K was also observed after processing and attributed to the plasticization effect provoked by triflusal molecules segregated in a molecular dispersion.

Particles of PMMA prepared by impregnation with triflusal presented a very slow release profile in both acid and basic media. Figure 4a shows the release profile in acid media, where it was found that 50% of the drug was released after 20 days. On the other hand, when individual pure triflusal was treated under similar experimental conditions, it was fully dissolved in a period of 15 min (Fig. 4b). The slow release of the sample indicated that the drug carried by the $SCCO_2$ was entrapped in the core of the particles and, hence, the long diffusion paths led to slow release of the drug.

L-PLA

It must be taken into account that highly crystalline polymers are seldom foamed by the pressure-induced process, since the sorption of gas occurs only in the amorphous region [40]. For the high molecular weight L-PLA polymer, the supercritical treatment was performed on the as-received pellets, which already had a high crystallinity and, as a consequence, a significant $SCCO_2$ foaming effect was not expected. On the other hand, semicrystalline polymers are seldom in thermodynamic equilibrium; hence, their state can be altered by a variety of treatments. It is generally acknowledged that in the presence of certain interactive liquids, crystallization of semicrystalline polymers can take place at temperatures well below the crystallization transition temperature of the polymer through a solvent-induced crystallization process [41]. The course of the induced crystallization starts with the sorption and diffusion of the diluent into the amorphous part of the polymer leading to the plasticization and an increase of free volume (swelling), which raises the rate of polymeric segmental motion by reducing the interchain interactions. Then, the process continues by the rearrangement of the molecules toward a crystalline condition. A similar effect is expected in a polymer $SCCO_2$-solvent induced crystallization process, since CO_2 at high pressure resembles common organic solvents in its ability to swell and plasticize polymers. The effect was studied in this work by annealing the high L-PLA molecular weight polymer at 323 K (near the glass transition temperature) and 393 K (near the melting temperature) under 12 MPa of CO_2 during 24 h. In the first case, a solvent-induced crystallization effect was expected, while in the second thermal-induced crystallization was more likely to occur.

Figure 5 shows a collection of L-PLA DSC thermographs. The thermograph from 310 to 490 K of the raw pellets showed two distinct endothermic thermal transitions. Firstly, a small peak that corresponds to the glass transition at 326 K. This was followed by a second sharp peak, related to the melting, at 463 K. The crystallinity of the raw L-PLA pellets was calculated to be 80%, relative to the enthalpy of melting for a enantiopure L-PLA of 100% crystallinity ($\Delta H_m^0 = 93$ J g^{-1}) [42]. Both the melting

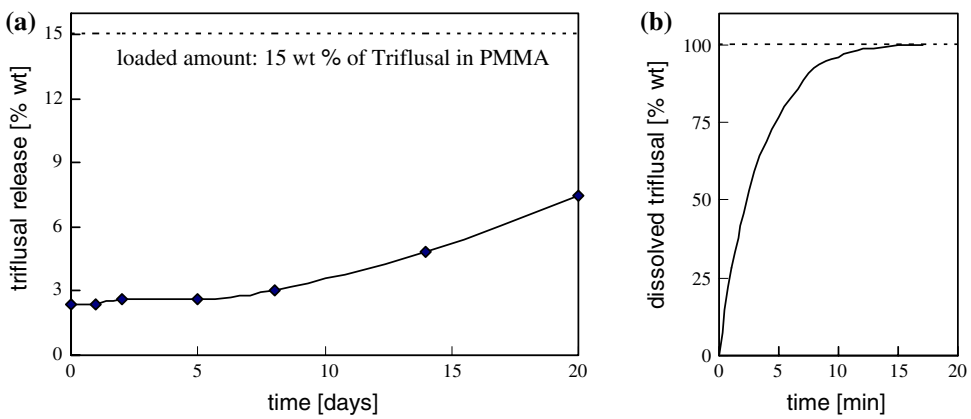

Fig. 4 (**a**) Profile of triflusal release in acid medium from impregnated PMMA (total loading 15 wt.% estimated by ^{1}H-NMR) and (**b**) raw triflusal dissolution in acid medium

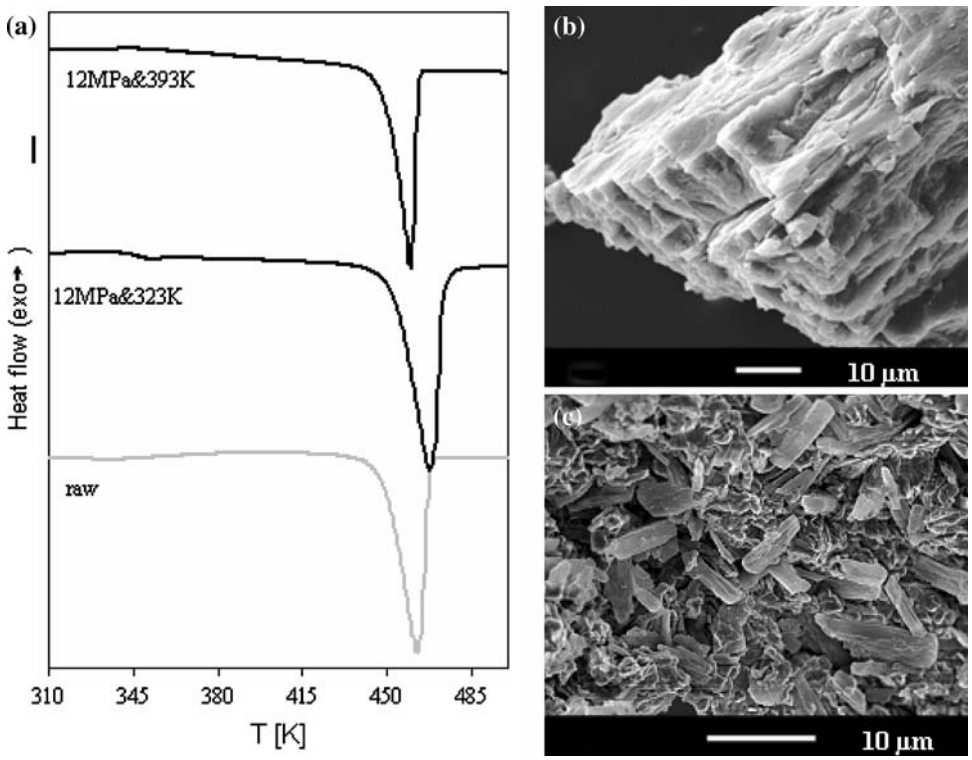

Fig. 5 (**a**) DSC thermograph of raw L-PLA pellets and treated during 24 h under $SCCO_2$ at 12 MPa and either 323 or 393 K, (**b**) SEM micrographs of L-PLA annealed under $SCCO_2$ at 12 MPa and 393 K, and (**c**) SEM micrographs of the mixture obtained after treating L-PLA with triflusal dissolved in $SCCO_2$ at 12 MPa and 323 K

enthalpy and the melting point increased after supercritical treatment at 323 K and 12 MPa. The crystallinity increased in about 4% and the T_m in 5 K, indicating a solvent-induced crystallization process well below the usual crystallization temperature of L-PLA (373–383 K).

Experiments indicated that further treatment under $SCCO_2$ at 12 MPa and 393 K enabled the raw L-PLA to fully crystallize as evidenced by an increase in crystallinity to 95% from the original value of 80% for the raw material. However, the $SCCO_2$ treatment at 393 K depressed the T_m in about 5 K. In the experiments carried out at 393 K, sample annealing involved both thermal and solvent energy input for crystallization. It was assumed that the rapid heat transfer in thermal-induced crystallization relative to diffusion mass transport in solvent-induced crystallization provoked that the L-PLA reacted to the input of sensible heat before any significant solvent penetration had taken place. The decrease in the melting point values indicated the formation of smaller crystals and a less organized crystalline structure in comparison to the raw materials. Since the polymer was initially highly crystalline, the formation of the less organized crystalline structure must be carried out through a recrystallization process, i.e., it first melts and then nucleates again. The melting happened because the interaction of the polymer with $SCCO_2$ lowered the effective T_m from the original values of 463 K at least up to 393 K. Upon $SCCO_2$ expansion at the end of the experiments, the melted samples experienced a sudden pressure and temperature drop, leading to a rapid re-association of the chain molecules. This provoked the rapid formation of nuclei and therefore the creation of small size spherulites and less organized crystalline regions. Although the melting temperature decreased for the treated sample, the melting enthalpy raised, indicating an increase of the degree of crystallinity with respect to the raw material.

The mechanical properties of lactic acid based polymers can be varied to a large extent ranging from soft and elastic plastics to stiff and high strength materials. Nanoindentation has been used in this work as a way to characterize the near-surface mechanical hardness of the used L-PLA polymer). Semicrystalline raw L-PLA had a hardness of 0.52 GPa measured using the nanoindenter. It was a ductile polymer at room temperature (below T_g) since it could endure a large amount of plastic deformation before fracture occurred. The hardness slightly increased to a value of 0.61 GPa after supercritical treatment at 323 K reflecting the solvent-induced crystallization effect. However, a significant decrease in hardness to a value of 0.12 GPa was observed after annealing at 12 MPa of $SCCO_2$ and 393 K. For this sample a brittle fracture mode was evident in the SEM photographs (Fig. 5b).

L-PLA was further processed under $SCCO_2$ conditions in the batch reactor at 12 MPa and 323 K, by adding to the polymer the same amount in weight of triflusal. SEM micrographs of the obtained sample (Fig. 5c) showed that the surface of the L-PLA polymer was covered of triflusal crystals. For semicrystalline polymers such as L-PLA, the induced nucleation and/or crystallization effect in the

L-PLA amorphous fraction prevented the dispersion of the drug in the matrix. The obtained formulation was a recrystallized drug particles embedded in the polymer matrix. During supercritical treatment at temperatures near the T_g, crystallization of the amorphous region of the L-PLA polymer occurred. Given that the crystalline L-PLA was not a swellable polymer any longer, it did not undergo triflusal impregnation and cannot be used as a drug delivery system.

Fibers precipitation experiments

The $SCCO_2$ swelled polymers did not have an interconnected porous geometry (see Fig. 2). Most of the described $SCCO_2$ foaming processes have been only able to attain on average 10–30% of interconnection between pores. Moreover, the small diameter of the pores often found using $SCCO_2$ foaming technology (from 0.1 μm to few μm) lead to pore occlusion by the living cells (with a few to tens μm in diameter). Finally, the porous structure of monolithic polymers obtained by pressure quenching make very difficult an effective seeding with cells due to their tortuous matrices [15, 33, 40, 43]. Similar problems are found using organic liquids as a porogen when preparing the scaffold by the more conventional temperature quenching process [44]. Although obtained materials are not thoroughly adequate to distribute a high density of cells efficiently and uniformly throughout the scaffold volume, they have potential pharmaceutical applications as controlled drug delivery devices with drug relief characteristics depending on the pore morphology [45].

To overcome the difficulties derived from the use of monolithic foamed scaffolds, three-dimensional meshes of polymer fibers are nowadays one of the preferred tissue scaffolds [46, 47]. The use of polymer fibers for biomedical and tissue engineering applications has some intrinsic advantages from a biomimetic approach, since a great variety of natural biomaterials are found with fibrous forms or structures (silk, keratin, collagen, cellulose, chitin, etc.). Therefore, polymer fibers can provide a proper route to emulate a biosystem such as the extracellular matrix. The results presented in this work are part of an ongoing work aimed to develop the possibilities of supercritical antisolvent precipitation technology for the precipitation of networks of fibers with an adequate architecture for tissue engineering applications.

The semicontinuous SAS equipment shown in Fig. 1b was used to produce fibers of the biopolymers. Basically, a

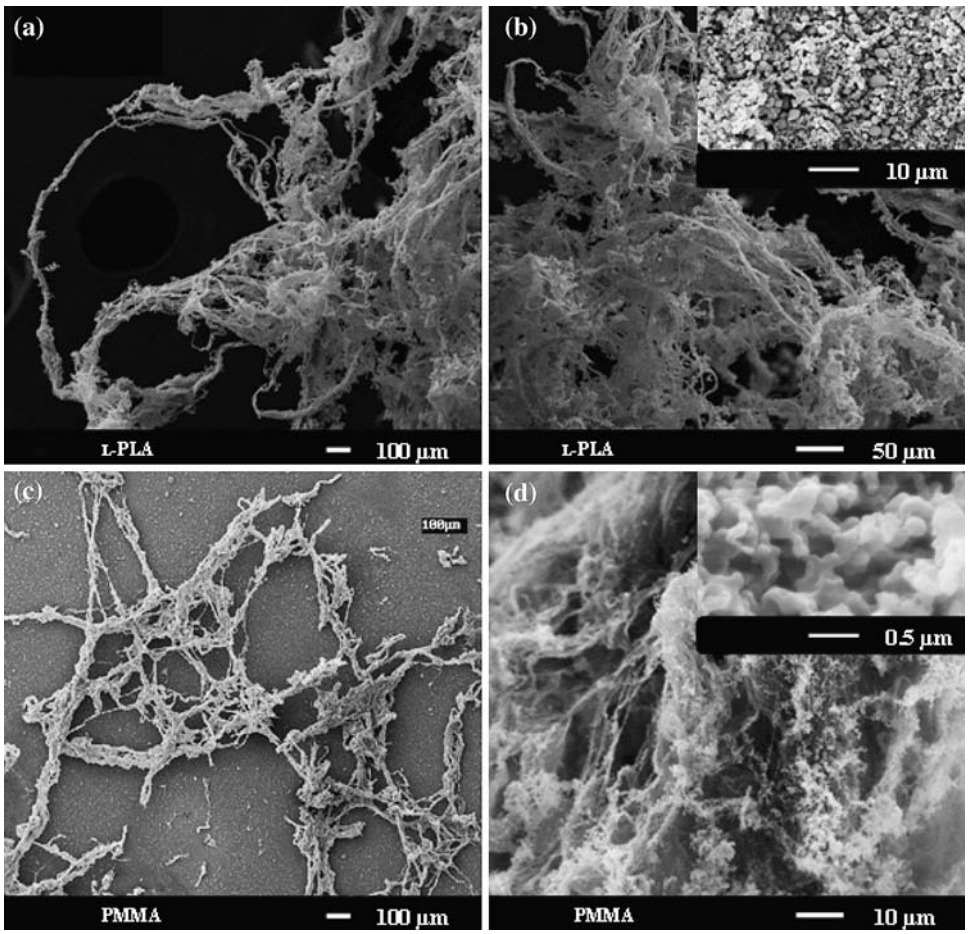

Fig. 6 SEM micrographs at different magnifications of polymer fibers obtained using the SAS process: (**a**, **b**) L-PLA at a polymer concentration of 2.8%, and (**b**, **c**) PMMA at a polymer concentration of 1.0%

homogeneous solution of the polymer to be precipitated was dissolved in DCM and was sprayed through an atomization device into a continuous $SCCO_2$ dense phase which played the role of the antisolvent. The simultaneous mass transfer of the dense gas and of the solvent from one phase to the other induced the supersaturation of the polymer, which precipitates. The results presented in this work clearly suggested that the SAS technique can be also used to process various biopolymers into fibers [48]. The obtained 3D network structures showed two different types of internal porosity. First, there was a macroscopic (several microns in diameter) porosity, observed in the SEM pictures Fig. 6a and b for L-PLA and PMMA fibers, respectively, formed by randomly oriented channels spread throughout the sample volume. Therefore, SAS prepared fibrous systems have a suitable macroporosity and interconnectivity to promote cell proliferation and to avoid pore occlusion by cell growth. Second, a continuous network structure of fused nanospheres composed the finest porosity of ca. 0.5–1 μm size (Fig. 6b, d). BET analysis showed that the fibers network have a high surface area of 60 $m^2\ g^{-1}$ for L-PLA and 250 $m^2\ g^{-1}$ for PMMA. Both samples presented meso and macroporosity (Fig. 7), although the total pore volume (between 10 and 1,000 Å) was higher for the PMMA network (0.17 $cm^3\ g^{-1}$) in comparison with the L-PLA sample (0.06 $cm^3\ g^{-1}$). Hence, the obtained scaffolds also exhibited adequate mesoporosity, necessary for capillary in-growth and neovascularization [1, 4].

The basic structure of these materials is made by small particles that either coalesced (for the L-PLA, Fig. 6c) or fused (for the PMMA, Fig. 6d), suggesting that experiments in this work were performed in a relatively dilute region, where the solid formation mechanism can be described by polymer nucleation and growth in a solvent rich phase [49, 50]. Coalescence of L-PLA particles seems limited to physical interaction, since the semicrystalline structure of the L-PLA difficulted agglomeration from plasticization. For the PMMA, the agglomeration and flocculation was extended in comparison with L-PLA due to its amorphous nature and $SCCO_2$ plasticization effect.

For both polymers, the morphological result is a rough textured surface with a high surface area to volume ratio. It should be taken into account that this is an essential requisite for effective cell seeding since it enhances cell adhesion onto the support [1, 4]. From a biomimetic approach, the obtained networks of polymer fibers had a morphology similar to that of natural collagen fibers [51].

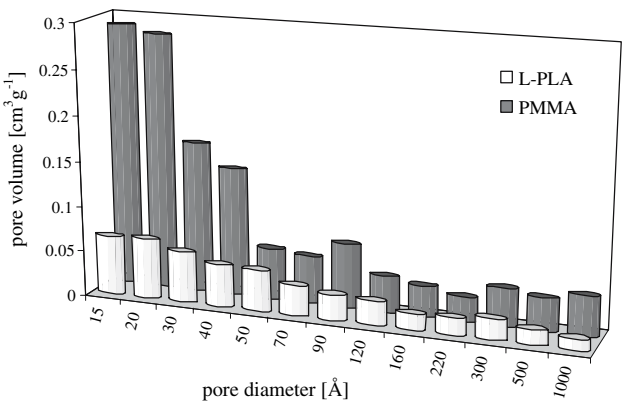

Fig. 7 Pore volume distribution versus pore diameter for L-PLA and PMMA fibers networks

Conclusions

The clinical success of a tissue construction is largely dependent on the quality of the starting scaffold. Macroporous sponges of the amorphous PMMA were fabricated using $SCCO_2$ as a porogen agent. This type of processing led to a partially closed pore structure, which is disadvantageous for cell-migration in 3D scaffolds. The development of new and versatile techniques for the production of clean and template-free polymeric fibers as an alternative to macroporous sponges represents a significant research interest. Fibers of PMMA and L-PLA homopolymers have been fabricated using the antisolvent SAS process.

Nonporous swellable matrixes are used as matrixes for controlled drug delivery. $SCCO_2$ was used here to plasticize and impregnate PMMA matrixes. Plasticization was accompanied by swelling with a consequent increase in the free volume of the polymer that was responsible for the enhanced diffusion of solute molecules in and out such systems. On the other hand, L-PLA is a semicrystalline polymer and it did not undergo impregnation to the molecular level, although its crystallinity was increased, that could lead to new applications of this material in tissue engineering of hard tissue.

Acknowledgements The financial support of EU Project STRP SurfaceT NMP2-CT-2005-013524 and the Spanish MEC (projects MAT2005-25567-E, MAT-2006-28189-E and MAT2005-25503-E) are greatly acknowledged. A. M. Lopez-Periago and C. A. García-González give acknowledgment to CSIC for its funding support through I3P fellowships.

References

1. Hutmacher DW (2000) Biomaterials 21:2529
2. Burg KJL, Porter S, Kellam JF (2000) Biomaterials 21:2347
3. Shin H, Jo S, Mikos AG (2003) Biomaterials 24:4353
4. Liu X, Ma PX (2004) Ann Biomed Eng 32(3):477
5. Whang K, Thomas CH, Healy KE, Nuber G (1995) Polymer 36:837
6. Zhang Y, Lim CT, Ramakrishna S, Huang Z-M (2005) J Mater Sci Mater Med 16:933

7. Tuzlakoglu K, Bolgen N, Salgado AJ, Gomes ME, Piskin E, Reis RL (2005) J Mater Sci Mater Med 16:1099
8. Cooper JA, Lu HH, Ko FK, Freeman JW, Laurencin CT (2005) Biomaterials 26:1523
9. Chen VJ, Ma PX (2004) Biomaterials 25:2065
10. Robinson JR, Lee VHL (1987) Controlled drug delivery: fundamentals and applications, 2nd edn. Marcel Dekker, New York
11. Beckman EJ (2004) J Supercrit Fluids 28:121
12. Tomasko DL, Li H, Liu D, Han X, Wingert MJ, Lee LJ, Koelling KW (2003) Ind Eng Chem Res 42:6431
13. Cooper AI (2000) J Mater Chem 10:207
14. Kazarian SG (2000) Polymer Sci Ser 42:78
15. Cooper AI (2003) Adv Mater 15:1049
16. Mooney DJ, Baldwin DF, Suh NP, Vacanti JP, Langer R (1996) Biomaterials 17:1417
17. Quirk RA, France RM, Shakesheff KM, Howdle SM (2004) Curr Opin Solid State Mater Sci 8:313
18. Howdle SM, Watson MS, Whitaker MJ, Popov VK, Davies MC, Mandel FS, Don Wang J, Shakesheff KM (2001) Chem Commun 1:109
19. Xu Q, Chang Y (2004) J Appl Polym Sci 93:742
20. Perrut M, Jung J, Leboeuf F (2005) Int J Pharm 288:11
21. Kazarian SG, Martirosyan GG (2002) Int J Pharm 232:81
22. Sheridan MH, Shea LD, Peters MC, Mooney DJ (2000) J Control Release 64:91
23. Kikic I, Vecchione F (2003) Curr Opin Solid State Mater Sci 7(4–5):399
24. Woods HM, Silva MCG, Nouvel C, Shakesheff KM, Howdle SM (2004) J Mater Chem 14:1663
25. Vega-González A, Domingo C, Elvira C, Subra P (2004) J Appl Polym Sci 91:2422
26. Reverchon E, Antonacci A (2007) J Supercrit Fluids 39:444
27. Thies J, Müller BW (1998) Eur J Pharm Biopharm 45:67
28. Randolph TW, Randolph AD, Mebes M, Yeung S (1993) Biotechnol Prog 9:429
29. Sproule TL, Lee JA, Li H, Lannutti JJ, Tomasko DL (2004) J Supercrit Fluids 28:241
30. Elvira C, Fanovich A, Fernandez M, Fraile J, San Roman J, Domingo C (2004) J Control Release 99:231
31. Muth O, Hirth Th, Vogel H (2000) J Supercrit Fluids 17:65
32. Condo PD, Johnston KP (1992) Macromolecules 25:6730
33. Üzer S, Akman U, Hortaçsu Ö (2006) J Supercrit Fluids 38:119
34. Kazarian S, Vincent MF, Bright FV, Liotta CL, Eckert CA (1996) J Am Chem Soc 118:1729
35. Wissinger RG, Paulatis ME (1987) J Polym Sci Part B Polym Phys 25:2497
36. Pantoula M, Panayiotou C (2006) J Supercrit Fluids 37:254
37. Goel SK, Beckman EJ (1994) Polym Eng Sci 34:1148
38. Barry JJA, Gidda HS, Scotchford CA, Howdle SM (2004) Biomaterials 25:3559
39. Krause B, Mettinkhof R, van der Vegt NFA, Wessling M (2001) Macromolecules 34:874
40. Sheridan MH, Shea LD, Peters MC, Mooney DJ (2000) J Control Release 64:91
41. Takada M, Hasegawa S, Ohshima M (2001) Polym Eng Sci 41:1938
42. Fischer EW, Sterzel HJ, Wegner G (1973) Colloid Polym Sci 251:1980
43. Nalawade SP, Picchioni F, Janssen LPBM (2006) Prog Polym Sci 31:19
44. Nauman EB, Ariyapadi MV, Balsara MV, Grocela TA, Furno JS, Liu SH, Mallikarjun R (1988) Chem Eng Commun 66:29
45. Baldwin SP, Saltzman WM (1998) Adv Drug Deliv Rev 33:71
46. Karageorgiou V, Kaplan D (2005) Biomaterials 26:5474
47. Moroni L, de Wijn JR, Blitterswijk CA (2006) Biomaterials 27:974
48. Bodmeier R, Wang H, Dixon DJ, Mawson S, Johnston KP (1995) Pharm Res 12:1211
49. Elvassore N, Baggio M, Pallado P, Bertucco A (2001) Biotechnol Bioeng 73:449
50. Dixon DJ, Johnston KP (1993) J Appl Polym Sci 50:1929
51. Gentleman E, Lay AN, Dickerson DA, Nauman EA, Livesay GA, Dee KC (2003) Biomaterials 24:3805